Multivariate geostatistical analysis of sedimentary infill in the Upper Salzach valley, Austria

Carmen JANDRISEVITS[1)*)], Robert MARSCHALLINGER[1)] & Thilo HOFMANN[2)]

[1)] Doctoral College GIScience, Interfaculty Department of Geoinformatics_Z-GIS,

University of Salzburg, Schillerstraße 30, 5020 Salzburg, Austria;

[2)] Department of Environmental Sciences, University of Vienna, Althanstraße 14 UZA II,

1090 Vienna, Austria;

[*)] Corresponding author, carmen.jandrisevits@sbg.ac.at

Abstract

The sedimentary infill of over-deepened alpine valleys and basins in the Eastern Alps are of great interest for groundwater resource management. The internal architecture and geometry of the sedimentary bodies within these valleys is generally complex, resulting in hydrological diverse groundwater systems. The objective of this study has been to model the 3D spatial distribution, sedimentary structures, and hydraulic properties of sediment infill in the Zell Basin of the upper Salzach valley (Austria). The irregular sample - spacing within the area, combined with the presence of highly unpredictable lateral extents of the sedimentary units, rendered 3D modeling of such complex sedimentary sequences a challenging exercise. Several possible geostatistical modeling/simulation approaches to developing realistic subsurface models of the heterogeneous sedimentary infill were investigated. Indicator kriging was found to smooth the spatial variability in stochastic simulations of a particular sediment type, and hence sequential indicator simulation, sequential indicator co-simulation, and multiple point statistics were used instead to simulate the 3D distribution of sedimentary units. Multiple point statistics was found to produce more realistic distributions than the variogram - based simulation methods, with better characterization of the lateral extent of sedimentary units.

Die Kenntnis von Sedimentfüllungen in übertieften alpinen Becken in den Ostalpen ist für das Grundwasserresourcen – Management von großem Interesse. Die interne Architektur und die Sedimentkörpergeometrien in diesen Becken sind generell komplex mit diversen hydrologischen Grundwasser - Systemen. Die vorliegende Studie untersucht die Sedimentstrukturen des Zellers Beckens im oberen Salzachtal. Ziel ist es, die 3D räumliche Verteilung von Sedimentstrukturen und zugehörigen hydraulischen Eigenschaften zu modellieren. Aufgrund der wenigen Eingangsdaten stellt die Modellierung von solch komplexen sedimentären Abfolgen eine Herausforderung dar. Verschiedene geostatistische Modellierung -/Simulationsverfahren wurden getestet, um realistische Untergrundmodelle der heterogenen Sedimentfüllungen zu erzeugen. Da mithilfe von herkömmlichen Interpolationsmethoden, wie Indikator Kriging die volle räumliche Variabilität von Sedimenttypen nicht abgebildet werden kann, kamen stochastische Simulationsverfahren wie Sequentielle Indikator Simulation, Sequentielle Indikator Co - Simulation und Mehrpunktstatistik zum Einsatz, um Realisationen der 3D Verteilung von Sedimenteinheiten zu simulieren. Im Vergleich zu den variogrammbasierten Simulationsmethoden können mittels Mehrpunktstatistik realistischere Modelle generiert werden, wo auch die laterale Ausdehnung von sedimentären Einheiten besser abgebildet werden kann.

1. Introduction

Valleys and basins that were over-deepened during the Quaternary glaciation are widespread in the Eastern Alps (e.g. Reitner, 2007; Brückl et al., 2010). The sedimentary structures and volumes of the valley and basin infill are of particular interest in applied geosciences, for groundwater resource management and for geotechnical projects (e.g. involving deep foundations and tunneling; Preusser et al., 2010), as well as being of interest for geomorphological and glaciological investigations (Fiebig et al., 2010). Full geological and hydrogeological characterization of the sedimentary inventory, however, requires a detailed description of its three-dimensional internal geometry (Webb, 1994). A complex sedimentary environment (such as that observed in the study area) may result in a highly heterogeneous spatial distribution of the hydrogeological parameter values in porous media at various scales (Klingbeil et al., 1999). These subsurface heterogeneities can never be explored in sufficient detail due to physical and financial limita-

tions on data collection. During recent decades numerous geostatistical approaches have been developed for assessing uncertainties in hydraulic properties. Stochastic modeling and simulations based on kriging (Krige, 1951) are state-of-art methods used for estimating multi-dimensional variability. Geostatistics is based on the theory of regionalized variables, i.e. variables that have both data values and locations in one-, two- or three-dimensional space. Variography is a traditional geostatistical method that is used to measure the spatial continuity of a regionalized variable based on the assumption that two points that are close together will have similar values because these values were generated under similar physical conditions (Isaaks and Srivastava, 1989). Kriging and kriging-based simulations require a variogram model to estimate or simulate the spatial distribution of a particular physical property at unsampled locations (Lark, 2000). Variogram analysis involves calculating an experimental variogram (the sample variogram)

from the data and fitting a variogram model to the sample variogram. The theoretical variogram model is chosen from a set of mathematical functions that describe spatial relationships. It shows the maximum variance or sill (C), and the correlation length. The sill is the sum of the nugget effect (C_0) and the spatial variance (C_1), i.e. $C = C_0 + C_1$. The nugget effect represents an apparent discontinuity at the variogram origin that is commonly attributed either to measurement errors or to geological structures with a correlation length shorter than the sampling resolution (Gringarten and Deutsch, 2001).

Kriging yields the best linear unbiased estimate ("BLUE") of a regionalized variable at unsampled locations and yields results that are considered to be locally accurate. It has a smoothing effect on the interpolated variable that results in small values being overestimated and large values being underestimated. Simulation is the process of producing multiple equally probable realizations of a regionalized variable. In contrast to kriging, which provides a single best estimate, simulation methods are globally accurate as they make use of two-point or multiple-point statistics that are representative of the area being investigated (Caers, 2000). Uncertainties can be assessed through alternative possible realizations, making simulations an appropriate tool for approximating the internal structure of sedimentary units (Webb, 1994). Sequential simulation (e.g. Gaussian simulation and sequential indicator simulation; Deutsch and Journel, 1998) is the most widely used stochastic simulation approach taken into account a given set of statistics, e.g. input data, histograms and variograms. Conditioning the simulation also honors sample data values at measured locations, i.e. the simulation is also locally accurate. The objective of this study was to compare the performance of conventional variogram-based geostatistical techniques, i.e. indicator kriging, sequential indicator simulation (SISIM; Deutsch and Journel, 1998), and sequential indicator co-simulation (COSISIM; Remy, 2004), with that of multiple point statistics (MPS; Strebelle, 2002), in order to assess their relative efficiencies in generating three-dimensional models of complex heterogeneous sedimentary bodies from sparse and spatially clustered input data. For our test site we investigated the upper Salzach valley, which is generally symmetrical and has an extremely heterogeneous sedimentary infill. There are no signs of extensive layering except within a shallow zone

that extends to a depth of 50 m, which has been interpreted as a pressured aquifer (Bleibinhaus and Hilberg, 2012). Geophysical and hydrogeological exploration has recently been carried out in the upper Salzach valley near Zell am See, prior to the construction of a hydropower plant. We simulated realizations, conditioned to hard and soft data to a depth of 50 m below surface, for an area of approximately 6 km² over the Zell Basin, in the upper part of the Salzach valley (Fig. 1). Drill log data are viewed by geostatisticians as "hard data" while indirect geophysical measurements are termed "soft data". The main objective of our study was to develop geologically different plausible 3D subsurface realizations of sediment bodies, with realistic geometric properties and boundaries. Different equally possible geological subsurface models will be used for numerical groundwater modeling. The most plausible subsurface model will be evolved by finding the best fit between the aquifers theoretical response and the measured hydrogeological data.

2. Study area and geological setting

The present-day Salzach River flows along the Salzach valley for a distance of approximately 250 km. In its upper section the river flows eastwards along the northern edge of the Tauern window, in a valley between the Hohe Tauern and the
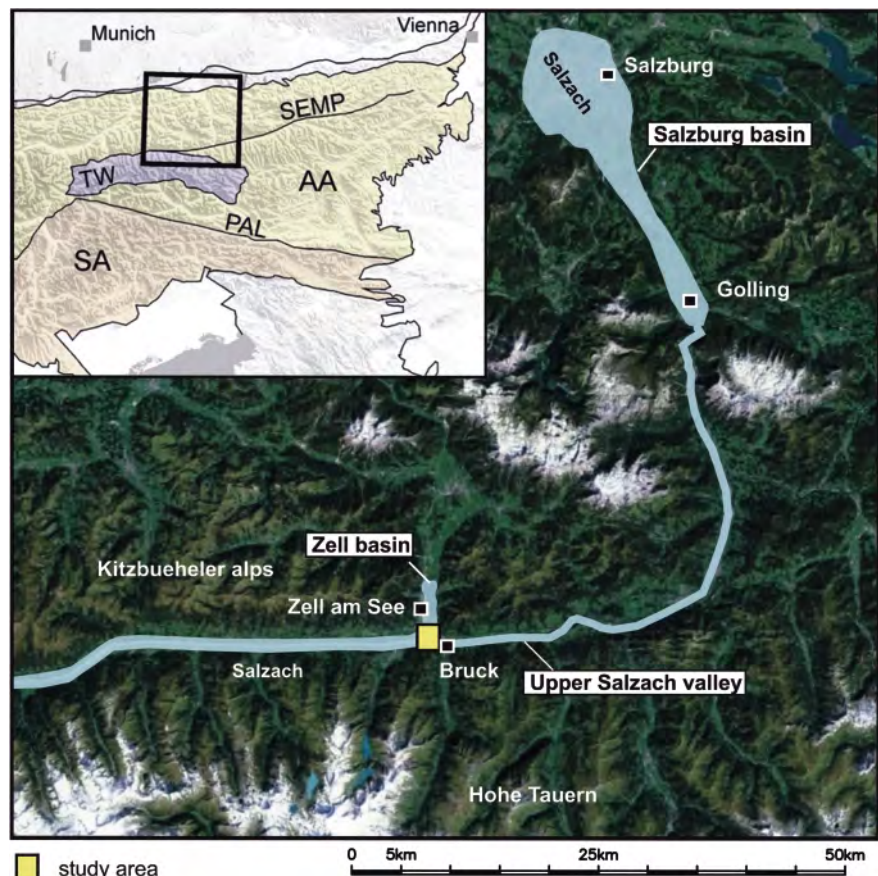

FIGURE 1: Location of study area in the Eastern Alps, on the northern edge of the Tauern Window (TW), and the drainage area of the Salzach River. The yellow rectangle shows the area of investigation. SA - South Alpine Unit; AA - Austroalpine Nappes; SEMP - Salzach-Ennstal-Mariazell-Puchberg Fault; PAL - Perdiadriatic Lineament.

Kitzbühler Alps. It then turns abruptly towards the north and cuts through the Northern Calcareous Alps into the Alpine foreland. To the north-east of Bruck, the Salzach valley cuts through the N-S orientated Zell Basin. The study area is located in the upper section of the Salzach valley, near Zell am See (Fig. 1). During the Quarternary the Salzach valley was covered by the Salzach glacier, which was the largest east Alpine piedmont glacier. The glacial ice in the upper Salzach valley during the last glacial maximum was at least 1500 m thick near the equilibrium line, and the ice surface reached an elevation of between 2000 and 2100 m (van Husen, 1987; Bleibinhaus and Hilberg, 2012). The regional dip of the ice surface was orientated towards the north, which meant that sediments were able to accumulate in the cross-cutting east-west oriented portion of the Salzach valley (Brückl et al., 2010; Bleibinhaus and Hilberg, 2012). Local ice markers indicate that the ice flow changed to the east of Bruck from an easterly ice-flow direction to a north-easterly direction (van Husen, 1987; Bleibinhaus and Hilberg, 2012). The Zell Basin was formed by the removal of sediments before they had time to consolidate (Bleibinhaus and Hilberg, 2012). Such over-deepened basins have been reported by van Husen (1979, 2000) to occur predominantly within the ablation area of glaciers. High ice velocities increase the debris load and the amount of glacial meltwater under hydrostatic pressure beneath the glacier. Apart from glacial erosion, tectonic subsidence has been suggested as another possible reason for the overdeepening since the

upper portion of the Salzach valley lies along the E-W striking Salzach-Enns-Mariazell-Puchberg Fault (Linzer et al., 2002). Sediment infill in the lower Salzach valley, or more precisely in the Salzburg Basin between Salzburg to the north and Golling to the south, has previously been reconstructed by van Husen (1979) from a cross-section based on shallow drill hole data and a number of deep drill holes. The maximum depth to bedrock in this over-deepened basin is approximately 330 m and the basin infill consists of moraines from the Würm ice age, overlain by silt and Holocene gravel and sand layers.

Geophysical surveys have been carried out by Bleibinhaus and Hilberg (2012) in the upper Salzach valley (Zell Basin), calibrated by drill hole data, in order to investigate sedimentary structures and the depth of the underlying bedrock. Interpretations of several 50 m deep drill log datasets suggested that the basin infill consisted mainly of sand, gravel, and discontinuous silt layers, indicating fluvial and occasionally lacustrine deposition.

Seismic refraction, electrical resistivity and ground penetrating radar surveys were conducted southwest of Zell am See. The results were interpreted as indicating the presence of a confined aquifer overlying a 150 m thick zone of unsaturated loose sediments. The great depth of the Zell Basin (approximately 480 m) was interpreted as probably due to the glacial erosion of tectonically weakened bedrock. The maximum age of the sediments in the upper Salzach valley was estimated to be less than 9 ka on the basis of ^{14}C data from peat ans wood layers in drill holes to the southwest of Zell am See, south to the Salzach River (Poscher, 1994).

3. Database and methods

3.1 Database

Our input data comprised drilling results and vertical profiles obtained from ground geoelectrical and geo-radar surveys, including spatial references and lithological information (Fig. 2).

Results are available from 56 drill holes within the area of interest, with depths ranging from 5 to 50 m. Drilling information was obtained from the underground utilities cadastre and from lithologic logs of 9 groundwater monitoring wells. From well logs the facies of sedimentary units in the study area have been established. By way of example, a well log profile is shown in Figure 3. The sedimentary infill mainly consists of gravel and sand and minor discontinuous silt/clay layers. Due to the sparse sampling density (see Fig. 2)
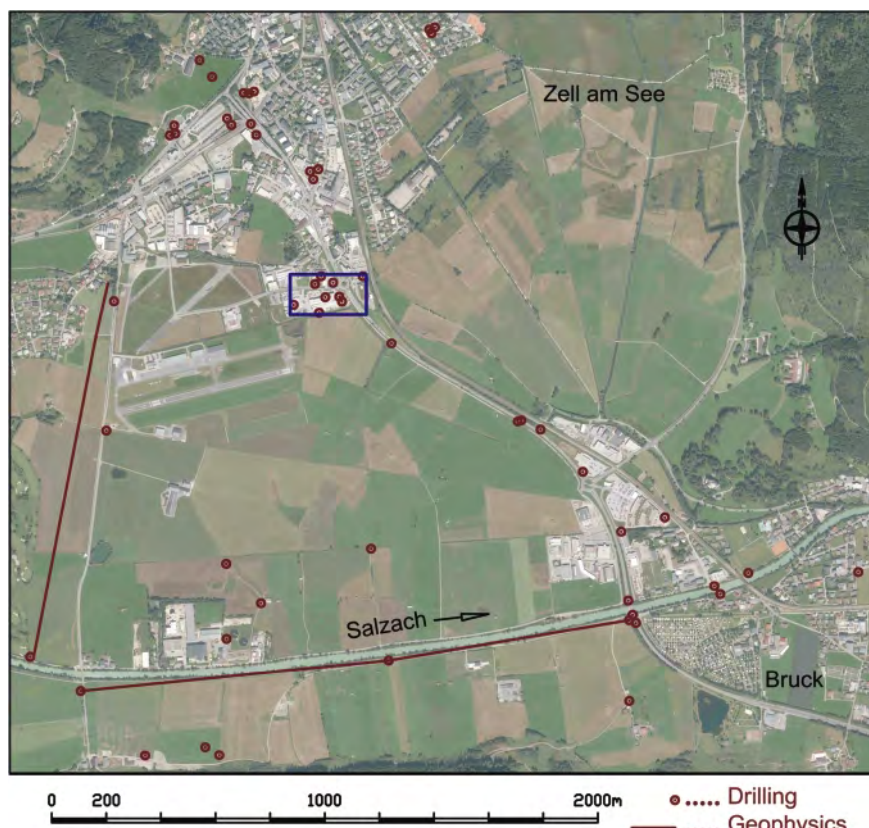

Figure 2: The entire study area with investigation data collection points (dark blue rectangle marks the central sub-area).

Drilling ○ .....
Geophysics — .....

0   200   1000   2000m

the 3D geometries of sediment facies and the transition from fluvial - lacustrine sedimentation are not clear.

Geophysical data were acquired in the form of a set of orthogonal (N-S and W-E) 2D profiles acquired in 2009 and 2010 for an improved understanding of the aquifer system (Fig. 2). Both profiles are approximately 2 km long and 50 - 70 m deep. Due to their hydrogeological properties three classes of lithology were distinguished: gravel, sand and silt/clay. In both profiles five significant horizons have been identified. For illustration a section of the W- E profile is shown in Figure 4. The W - E profile was interpreted from both resistivity sounding data and well information. The uppermost horizon extends to a depth of 2 – 4 m and is made up of dry gravel sediments. Below, a water bearing sand horizon with an average thickness of 10 m is identified. A silt/clay horizon of approximately 10 - 20 m thickness underlies the sand layer. Aquifer sands with a thickness of 15 - 30 m are partly laterally confined (0 – 900 m and 950 – 2000 m) between silt/clay layers. The bottom silt/clay horizon is approx. 20 - 30 m thick. By combining seismics, geoelectrics, ground penetrating radar and well data, N-S orientated profile of the Upper Salzach valley has been conducted. Bleibinhaus and Hilberg (2012) give an interpretation of the N-S profile. In the central and southern part of the cross section a highly resistive 5 m thick sand layer builds the upper horizon. Below a 10 m thick silt layer is identified followed by a 15 m thick zone of pressured aquifer sands in the center of the section. Interpretation of well data suggests that the aquifer is confined whenever a silt layer is on top. Next to the Salzach, well data indicate unpressured groundwater at shallow depth that probably drains into the river. Well data show a widespread silt- covering layer probably due to a sizeable late postglacial lake. The continuity of the silt/clay covering layer is interrupted by the present and former paleo river bed.

3.2 Analysis Method

Drilling information from within the investigated area has previously been interpreted and classified by different researchers, so it was necessary to combine the various detailed classifications. To this end we distinguished three different classes on the basis of their hydraulic properties (Table 1). In Figure 5 drillings, showing the vertical extent of the three sediment facies, are visualized for the investigated subarea and the entire study area.

In the discussions below Class 0 is referred to as "gravel", Class 1 as "sand", and Class 2 as "silt/clay". Geostatistical data analysis, together with indicator-based interpolations and simulations, were accomplished using the Geostatistical Software Library (GSLIB) and Stanford Geostatistical Earth Modeling Software (SGeMS).
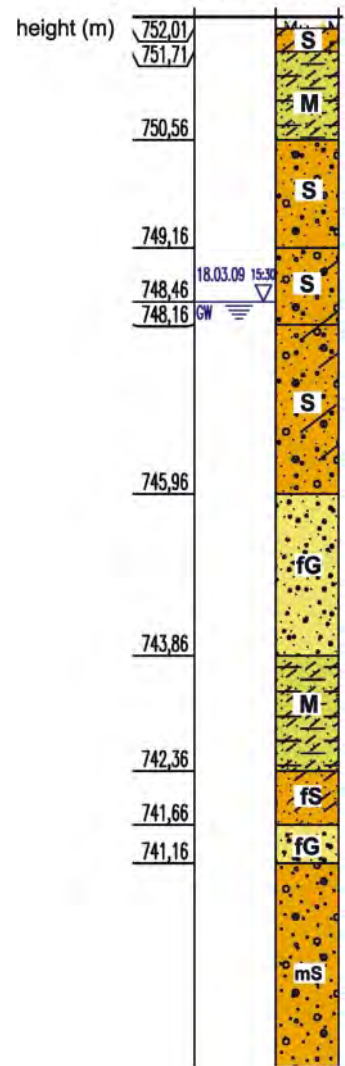

FIGURE 3: Log profiles of one borehole. fG: fine gravel, S: sand, fS: fine Sand, mS: middle Sand, M: Silt.
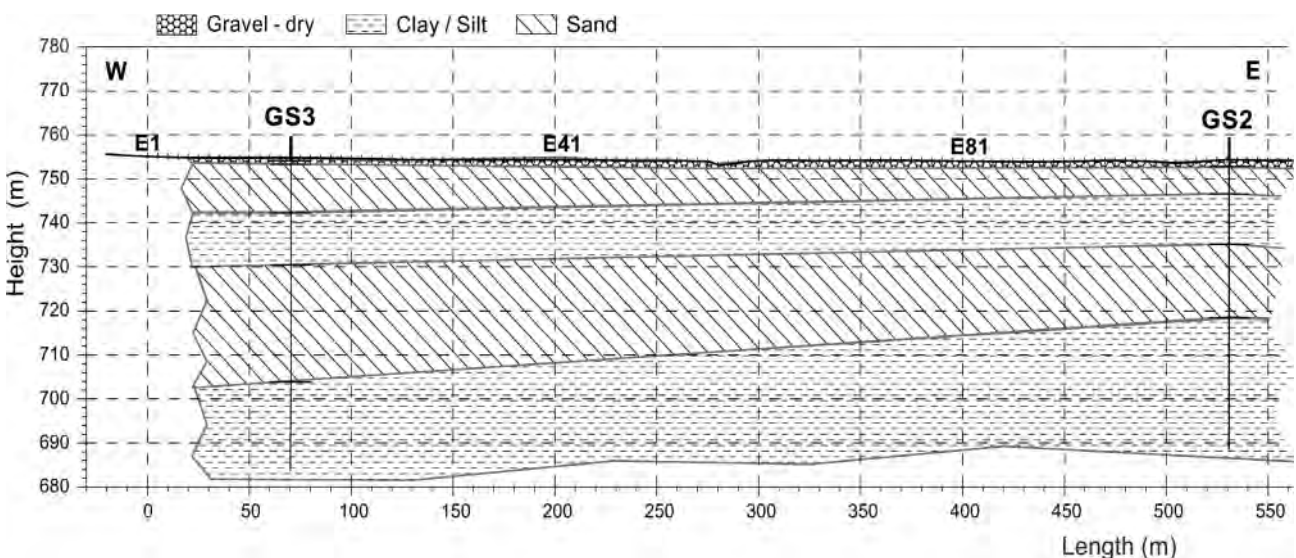

FIGURE 4: Part of W-E cross-section and the sequence of sediments described in the text. For the location of the profiles see Fig. 2.

Class	0	1	2
Hydraulic conductivities	kf: $5 - 10^{-2}$ m/s	kf: $10^{-2} - 10^{-6}$ m/s	kf: $10^{-6} - < 10^{-9}$ m/s
Sediment facies	Boulders, Stones Coarse Gravel Medium Gravel Fine Gravel	Coarse Sand Medium Sand Fine Sand	Silt Loam Clay

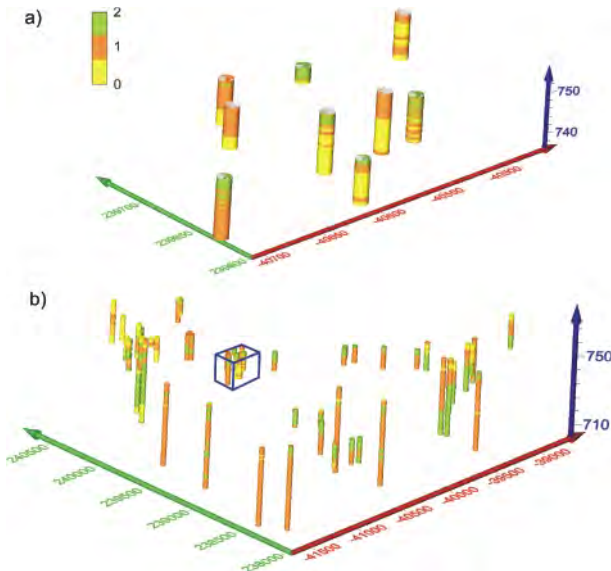**TABLE 1:** Sediment facies classification.

FIGURE 5: (a) Visualization of drillings according to sediment classification in Tab.1 (0 = "gravel", 1 =" sand", "2" =silt/clay) for the central volume (three-fold vertical exaggeration) and (b) for the entire volume (cuboid outlines the subarea) (ten – fold exaggeration).

3.3 SEQUENTIAL INDICATOR SIMULATON (SISIM) AND INDICATOR KRIGING (IK)

The sequential indicator simulation technique uses an indicator formalism introduced by Switzer (1977). Geostatisticians at the Standford Center for Reservoir Forecasting (SCRF) developed this non - Gaussian algorithm in order to characterize three-dimensional uncertainty in reservoir models (Journel and Albert, 1989; Deutsch and Journel, 1998). Sequential indicator simulation relies on indicator kriging and is capable of working with both thresholded continuous variables and categorical variables (e.g. soil types). The categorical information is defined as one of z_k possible states, where $k=1... K$. Both continuous and categorical data are nonlinearly transformed into binary variables. The indicator variable is set to 1 for locations with specific facies data and to 0 for locations where the facies type is not available (Deutsch and Journel, 1998):

$$I(u; z_k) = \begin{cases} 1; if\ z(u) = z_k \\ 0;\ otherwise \end{cases}$$

Indicator kriging uses indicator-transformed values. For thresholded continuous variables indicator kriging yields an estimate of the cumulative distribution function, based on the behavior and correlation the indicator-transformed data (Journel, 1983).

Categorical variables are used to directly estimate the probability of occurrence (distribution of uncertainty) in the categorical facies variable. The probability distribution consists of estimated probabilities for each category. The spatial correlation is described by a variogram. For a specific category $\gamma I(h, z_k)$ the variogram is defined as the mean quadratic increment between two indicators (I) separated by a lag distance h.

$$\gamma I(h, z_k) = \frac{1}{2N(h)} \sum_{1}^{N(h)} [I(u; z_k) - I(u+h, z_k)]^2$$

The gamv module in the GSLIB package (Deutsch and Journel, 1998) was used to compute 3D variograms from the irregularly spaced data for variogram computation from the irregularly spaced data in three dimensions. Variogram values for each class were calculated from the transformed (i.e. "0 to 1") dataset. Full indicator kriging requires a variogram model for each z_k class. A three-dimensional variogram interpretation is required to achieve a full description of the geological continuity (Gringarten and Deutsch, 2001). Vertical and horizontal variograms were first computed in different directions and for different inclinations, in order to then produce a realistic 3D variogram model. Due to a higher sampling frequency in the vertical direction, shorter vertical lag distances were used in calculating the vertical sample variogram. The total variability (or sill) in the direction of the highest variance is given by the sum of the variance contributions of the nested structures (combination of horizontal and vertical variogram models) and the nugget effect. The variograms for "sand" are shown in Figure 6 by way of an example. Variogram parameters for the different classes are shown in Table 2. The correlation scale in the vertical direction was determined by fitting a spherical model to the variograms for each class. This spherical model showed a sharp increase and then quickly levelled off, rendering this model suitable for portraying abrupt geometrical change. Horizontal variograms were fitted with an exponential model that increased gradually and approached the sill asymptotically. There was a geometric anisotropy in the variogram behavior, with a shorter range of correlation in vertical directions than in horizontal directions. Comparing the variograms revealed that the horizontal variogram also encountered a zonal anisotropy as it did not reach the total variability.

Sequential use of indicator kriging aims to reproduce multivariate properties conditioned to sampled data. The SISIM code, a sequential indicator simulation algorithm, realized in GSLIB (Deutsch and Journel, 1998) and SGeMS (Remy et al., 2009) packages, was used for conditional simulation of sedimentary facies.

The sequential simulation procedure for categorical variables involved the following steps:

1. Defining a random path on the simulation grid, visiting all unsampled locations.

2. For each grid location $u = 1, …, N$,

    a) determining the local conditional distribution using the original data and previously simulated data,

    b) drawing a random number from the cumulative distribution function ϵ [0,1] and adding it to the simulated (conditioning) data, and

    c) finding which category was specified by the number k and assigning category k to location u.

3. Repeating the above until all nodes on the simulation grid had been simulated.

Multiple realizations were obtained by repeating the entire sequential generation process using different random paths. Sequential indicator simulations were conditioned to existing hard data across the study area.

FIGURE 6: Vertical and horizontal variograms and models for the "sand" class.

3.4 SEQUENTIAL INDICATOR CO - SIMULATION

The COSISIM algorithm extends the SISIM algorithm to handle secondary (soft) data (Remy, 2004). Soft data were integrated with hard data using the Markov-Bayes algorithm (Deutsch and Journel, 1998; Zhu and Journel, 1993). As with the primary attributes (hard data), secondary information must be coded into indicators before it can be used. The indicator-coded soft data can be interpreted as a secondary variable (Y) and accounted for by solving the cokriging system. The cokriging estimator is given by

$$I^{*}(u, z_k) = \sum_{\alpha} \lambda_{\alpha} I(u_{\alpha}; z_k) + \sum_{\beta} \lambda_{\beta} Y(u_{\beta}; z_k)$$

with $Y(u\beta, zk) = F^{*}(Z(u) \leq zk|Y)$ and F^{*} as the conditional prior distribution function. The λ_{α} values relate to weightings assigned to neighboring hard data and the λ_{β} values relate to weightings assigned to neighboring soft data. Solving the cokriging system requires a knowledge of the covariances of hard and soft data, and of the cross covariances between hard and soft data. In reality, however, there is usually insufficient data (hard and soft) for all indicator covariances to be precisely inferred. To overcome this drawback the following Markov hypothesis (or approximation) is used. It states that hard information $I(u;z)$ screens any soft collocated information $Y(u;z)$ in the sense that:

$$Prob\ (Z(u') <= z_k | i(u, z_k), y(u, z_k)) = Prob(Z(u')$$
$$\leq z_k | i(u, z_k)\ \ \forall u, z_k$$

Under this assumption the covariance of the soft data CY (h, z_k) and the cross covariance between hard and soft data CIY (h,z_k) are calculated as follows (Deutsch and Journel, 1998):

$$CY(h, z_k) = \begin{cases} |B(z_k|CI(h, z_k)\ \ if\ \|h\| = 0 \\ B(z_k)CI\ (h, z_k)\ \ if\ \|h\| > 0 \end{cases}$$

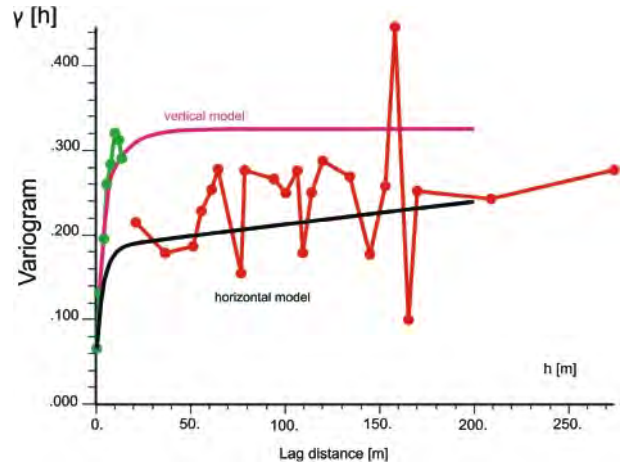| Class	Nugget	Sill	Variance contribution	Type of variogram	Max. horiz. range [m]	Min. horiz. range [m]	Vertical range [m]
0 (Gravel)	0.06	0.325	0.14	Spherical	750	750	8
			0.125	Exponential	30	6	12
1 (Sand)	0.05	0.33	0.09	Spherical	1000	1000	3
			0.19	Exponential	15	15	25
2 (Silt/Clay)	0.01	0.274	0.184	Spherical	300	300	12
			0.08	Exponential	25	10	12

TABLE 2: Variogram parameters.

$$CIY(h, z_k) = B(z_k)CI\ (h, z_k)$$

The hard covariance model CI (h,z_k) can be derived from the semivariogram of the hard data. By using the $B(z)$ coefficient the soft covariance model and cross covariance model can then be determined. The value of $B(z)$ can be in the range between -1 and $+1$: it regulates the influence of soft data on estimation results. If $B(z) = 1$ soft data are treated equally with hard data and if $B(z) = 0$ soft data are neglected (Sil et al, 2008). Updating of the prior probabilities Y ($u; z_k$) under a Markov hypothesis is referred as the "Markov-Bayes algorithm" (Remy, 2004).

3.5 MULTIPLE POINT STATISTICS

Multiple point statistical (MPS) techniques were developed in the field of petroleum engineering because two-point spatial correlation functions and traditional variogram models do not allow modeling of the curvilinear or geometrically complex patterns observed in hydrocarbon reservoirs (Strebelle, 2000, 2002; Zhang et al., 2006). The method has been successfully applied in variety of case studies, such as for modeling complex sedimentary facies in fluvial (Strebelle and Zhang, 2004) and turbiditic (Strebelle et al., 2003) systems. Instead of a variogram, MPS incorporates a user-supplied training image (TI) that provides a conceptual description of the subsurface geological heterogeneity and contains the major patterns of the subsurface geology (Strebelle, 2002). As such, the TI over-

comes the limitations of classical variogram-based (2-point) geostatistics, by searching for multiple-point correlations in order to characterize the spatial structure, thus allowing the reproduction of complex patterns (Strebelle and Journel, 2001). The definition of an adequate training image is a crucial and difficult part of the MPS approach. Training images can be generated using different data sources such as images of outcrops, geological scetches or physical-based models. A three-dimensional TI of the study area was generated using the Tetris object-based training image generator in the SGeMS software. The TI represents a reference facies model for a subarea of the entire investigation area that depicts the depositional patterns and the three-dimensional variability of sediment facies types. Figure 7a shows the TI for the three sediment classes. The lateral dimensions and spatial variability of sediments formed by glacial activity were estimated using satellite imagery for the glacier foreland of the Pasterze Glacier (Hohe Tauern, Austria) in the Eastern Alps. The imagery provided a recent example of the proglacial fluvial and lacustrine sedi-
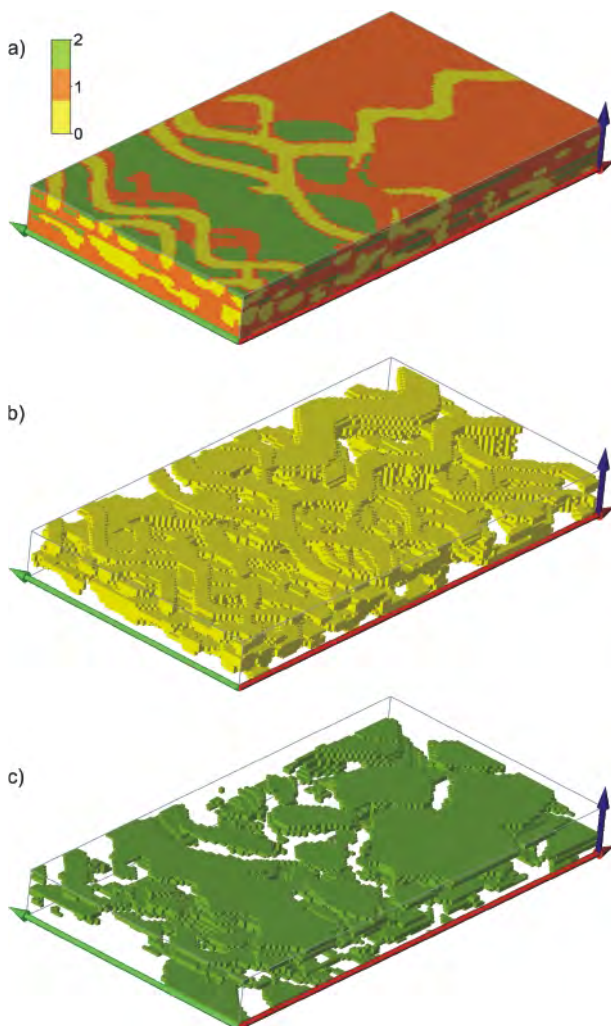
mentary processes observed in many Alpine valleys and Alpine forelands during Quaternary glaciation. Krainer and Poscher (1992) investigated the sedimentary characteristics along deglaciated foreland of the glacier. A small periglacial valley sandur has formed as a result of the rapid retreat of the Pasterze Glacier during the last few decades. This outwash plain of valley sandur is characterized by a braided stream system composed of various channels and different types of bars. The channel widths can be in excess of 5 m and the dominant lithofacies are coarse gravels and boulders. Kettle-hole lakes with diameters of up to 7 m occur in the proximal part of the glacier foreland. A shallow glacial lake is dammed up on the distal part of the valley sandur during the summer months. In the TI gravel deposits were modeled as sinusoidal bodies (Fig. 7b). Fine-grained glacial lake deposits such as silt and clay were modeled as half-ellipsoid bodies (Fig. 7c). The rest of the volume of the TI was made up of sand sediments. The vertical extent of sediment bodies was modeled to match their vertical extent in drill-log sections. The proportions of the vari-
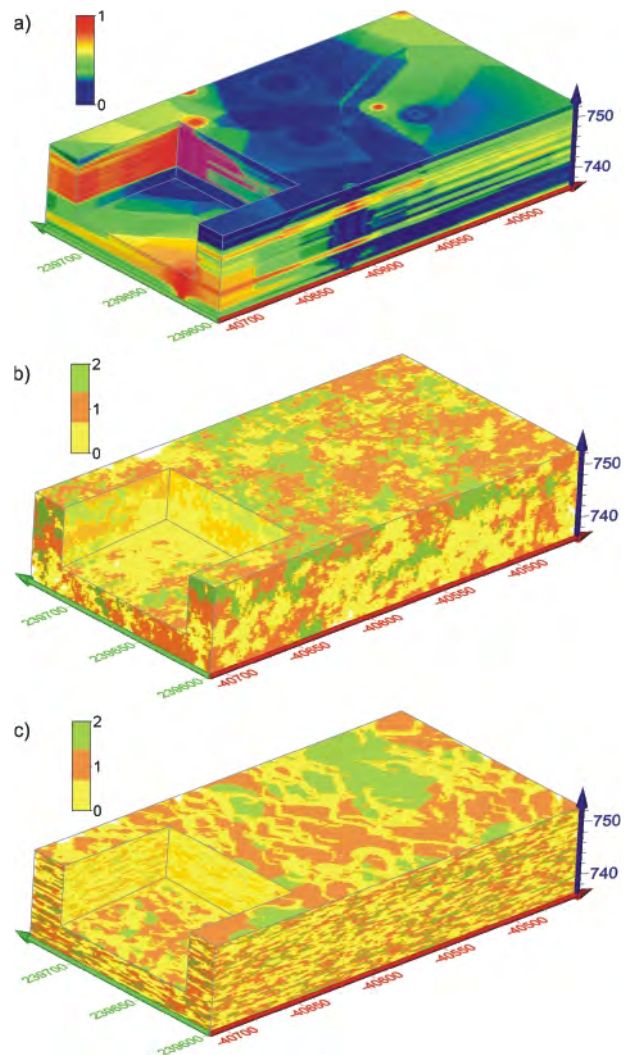

FIGURE 7: (a) Training image with volume dimensions x = 127 m (red axis), y = 67 m (green axis), z = 4.4 m (blue axis) (three-fold vertical exaggeration). (b) Channel structures of the coarse-grained material which is predominantly gravel (class 0). (c) Half-ellipsoid structures of the fine-grained (silt/clay) sediments (class 2).

FIGURE 8: (a) IK model for "sand" (red zones (1) show very high probabilities, while blue zones (0) indicate very low probabilities) and randomly selected simulated volumes, with (b) SISIM and (c) SNESIM for the central volume (3-fold vertical exaggeration).

ous lithofacies in the TI were assumed to be the same as their proportions in the drill holes.

MPS simulations reproduce spatial patterns from TIs while also conforming to conditioning drill hole data. Facies models within the study area were simulated using the Snesim (Single Normal Equation SIMulation) algorithm (Strebelle, 2000, 2002) implemented in SGeMS software. SNESIM is a pixel-based algorithm that has a similar basis to sequential indicator simulation, in which each grid cell facies is sequentially simulated along a random path and the simulation of cells later in the process is constrained by the cells already simulated earlier in the process (Caers and Zhang, 2002).

4. Results and discussion

The geostatistical calculations were performed on two different domains (Fig. 2):

1. A "central volume" (x = 254 m, y = 134 m, z = 17 m) whose surface area is outlined by the dark blue rectangle in Figure 2, was discretized with fine grid cells (1 m × 1 m × 0.2 m).

Class	Input proportion	SISIM	SNESIM
0 (Gravel)	40%	39%	40%
1 (Sand)	45%	43%	45%
2 (Silt/Clay)	15%	18%	15%

Table 3: Input and output proportions of sediment classes in the central volume.

This volume was chosen in the area with the highest density of conditioning data (Fig. 5a).

2. The "entire volume" (x = 3040 m, y = 2680 m, z = 69 m) covering the surface area displayed in Figure 2 was discretized with a coarse grid (10 m × 10 m × 1 m). Conditioning drillings are shown in Fig. 5b).

4.1 Central volume

IK, SISIM and SNESIM were performed on the central volume. Classes were calculated by means of IK probability models of sediment facies. Figure 8a shows the probability mo-
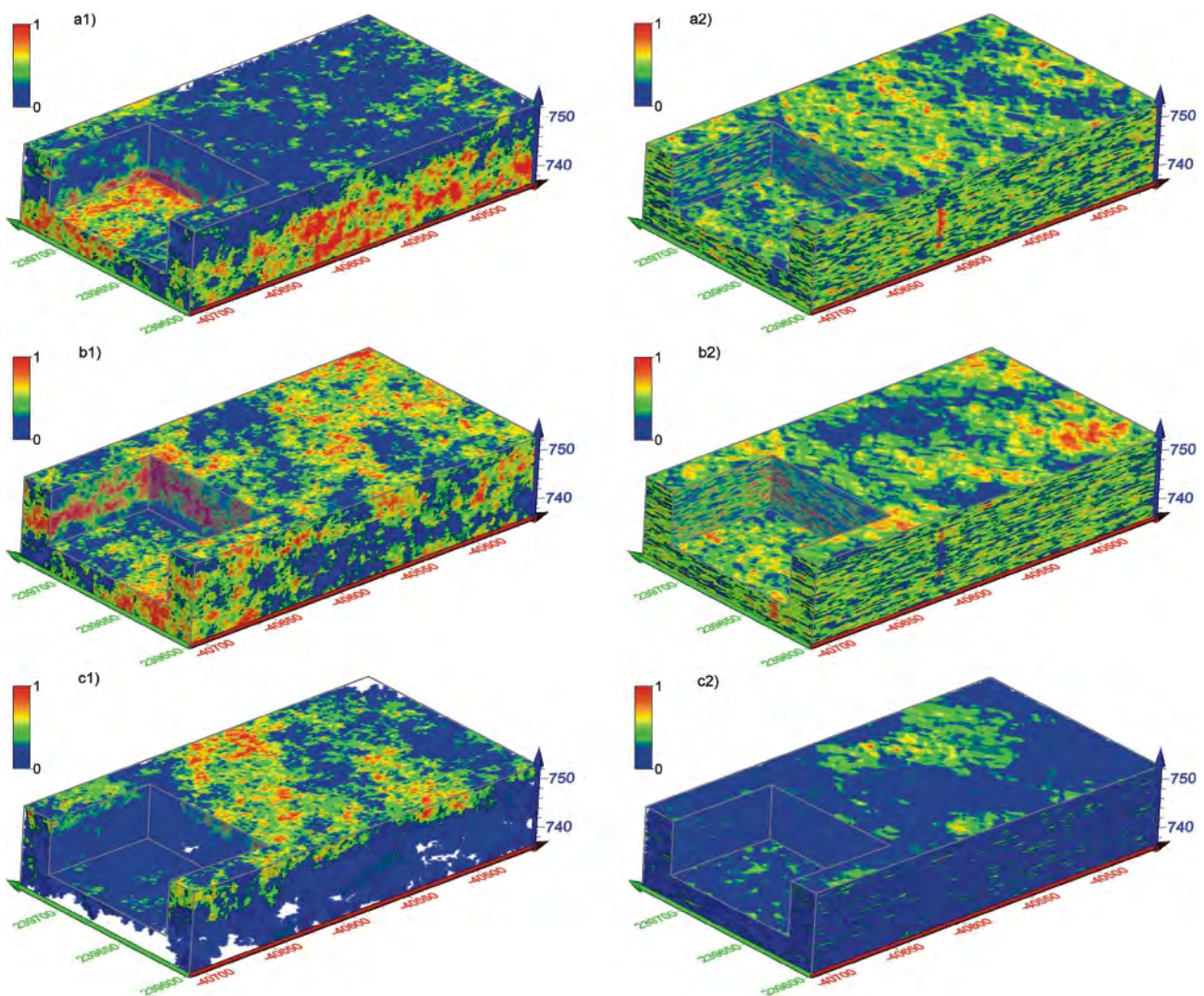

Figure 9: Probability of finding each sediment class for the entire volume with SISIM:.(a1) "gravel"; (b1) "sand"; (c1) "silt; and with SNESIM: (a2) "gravel"; (b2) "sand"; (c2) "silt" (3-fold vertical exaggeration).

del for "sand". The lateral extent of each sediment class in the model is strongly influenced by the search geometry in the IK interpolation. The smoothing characteristics of IK are clearly evident. From a geological point of view IK yielded an accurate estimate of sediment facies probability for positions close to the drill hole locations, but it yielded an increasingly unrealistic picture as the distance from the drill holes increased, due to the absence of any conditioning data.10 equally probable realizations were obtained using SISIM and SNESIM. A randomly selected simulation obtained using SISIM is shown in Figure 8b and an SNESIM realization is depicted in Figure 8c. SISIM yielded a good approximation of the original facies proportions. Facies transition zones in the SISIM model were, however, not geologically realistic, with patchy and unstructured appearances. The shapes of sediment bodies and facies continuity were depicted more realistically by SNESIM than by SISIM. Local conditional probabilities were corrected by means of the servosystem implemented in the SNESIM algorithm (Boucher, 2013), so that output proportions in the final realization accurately reproduced the input proportions.

The probability of occurrence for every sediment class was computed from the 10 equally probable realizations from the SISIM (Fig. 9a1 b1 c1) and SNESIM (Fig. 9a2 b2 c2) models. The SNESIM model produced laterally persistent sediment bodies whose shape and size were similar to those depicted in the training image. Channel-like structures that were modeled in the TI and in the SNESIM models are not present in the
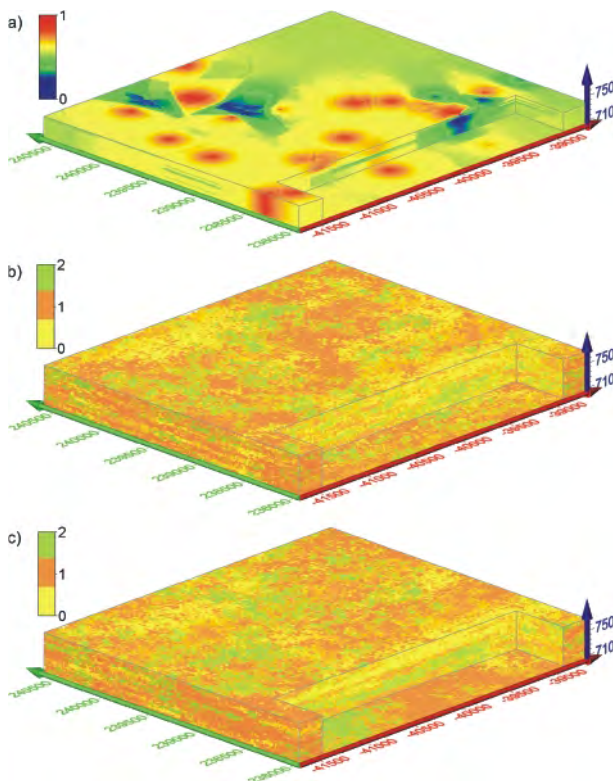
SISIM models.

4.2 Entire volume

IK, SISIM and COSISIM models were computed for the entire volume. Facies input proportions were different from those for the central volume. According to the hard data 17% of the volume belonged to the "gravel" class, 52% to the "sand" class, and 31% to the "silt/clay" class. Figure 10a shows the IK model for the "sand" class. The density of drill holes over the entire volume is lower than over the central volume and since those drill holes that do exist are irregularly distributed, IK does not allow any reproduction of spatial variations in sediment facies. Concentric shapes around drilling locations are due to the influence of the search ellipsoid geometry. As was the case for the central volume, SISIM gave a better insight into the spatial variability but did not provide any information on the lateral extent of sedimentary units (Fig. 10b). Two 2D geoelectric sections were integrated using COSISIM, in addition to the drilling data. A clearer facies concentration is observed in certain parts of the simulation model than in others, due to the influence of the geoelectric sections (Fig. 10c).

5. Conclusion

In this study we have tested different geostatistical interpolation and simulation methods to create realistic 3D models of the heterogeneous sedimentary infill in the Zell Basin of the upper Salzach valley. Where investigation data was scarce geostatistical interpolation (i.e. indicator kriging) was unable to reveal the spatial variations in sediment types, and conditional stochastic simulation methods were more appropriate for modeling spatial variability. Our study clearly showed that variograms are unable to capture the facies heterogenity found in complex sedimentary settings: the simulation realizations did not provide a realistic description of the spatial variability with plausible and interpretable shapes for the sedimentary bodies. Simulations conditioned by data from drill holes and geophysical surveys allowed the prediction of the lateral extent of sedimentary units. A complete and accurate representation of sedimentary units over the entire investigation area would, however, require more detailed geophysical data and interpretations.

Compared to variogram-based interpolation and simulation methods, multiple point statistics was found to be the most powerful approach for describing the spatial structure and geometric shapes of complex sedimentary units. The 3D training image offered a very efficient way of modeling complex sedimentary bodies as it allowed the incorporation of geological information concerning shape and depositional/erosional processes. Future modeling will therefore focus on the multiple point statistics approach. Multiple point statistical simulation conditioned to both hard and soft data will be used for improving subsurface models of subarea and entire investigation area. Multiple simulated facies realizations will be used as input to a groundwater flow model. The influence of different geological scenarios on the groundwater flow will be compa-

Figure 10: (a) IK model for "sand" (red zones (1) show very high probabilities, while blue zones (0) indicate very low probabilities) and randomly selected simulations with (b) SISIM and (c) SNESIM for the entire volume (five-fold vertical exaggeration).

red to evaluate the different geological scenarios, ending up with most plausible and realistic subsurface realization.

REFERENCES

Bleibinhaus, F. and Hilberg, S., 2012. Shape and structure of the Salzach Valley, Austria, from seismic traveltime tomography and full waveform inversion. Geophysical Journal International, 189, 1701-1716.

Boucher, A., 2013. Multiple Point Geostatistics: Modeling with Training – Image based algorithms. Course material.

Brückl, E., Brückl, J. Chwatal, W. and Ullrich, C., 2010. Deep alpine valleys—examples of geophysical explorations in Austria. Swiss Journal of Geosciences, 103 (3), 329-344.

Caers, J., 2000. Direct sequential indicator simulation. In: Kleingeld, W.J. and Krige, D.G. (eds.), Geostats 2000 Cape Town, 1, pp. 39-48.

Caers, J. and Zhang, T., 2002. Multiple-point geostatistics: a quantitative vehicle for integrating geologic analogs into multiple reservoir models. In: G.M. Grammer, P.M. Harris and G. P. Eberli (eds), Integration of Outcrop and Modern Analogs in Reservoir Modeling. American Association of Petroleum Geologists, Memoirs, pp. 383-394.

Deutsch C.V. and Journel A.G. ,1998. GSLIB, geostatistical software library and user's guide. Oxford University Press, New York, 369 pp.

Fiebig, M., Preusser, F., Decker, K. and Schlüchter, C., 2010. Preface: special section of papers dealing with overdeepened basins and valleys in the alpine realm. Swiss Journal of Geosciences, 103(3), 327-328.

Gringarten, E. and Deutsch, C., 2001. Teacher's aide variogram interpretation and modeling. Mathematical Geology, 4, 507-534.

Husen van, D., 1979. Verbreitung, Ursachen und Füllung glazial übertiefter Talabschnitte an Beispielen in den Ostalpen. (Distribution, Reasons, and Refill of Glacially Deepened Valley-Sections by Examples of the Eastern Alps.). Eiszeitalter und Gegenwart – Quarternary Science Journal, 29, 9-22.

Husen van, D., 1987. Die Ostalpen in den Eiszeiten (The Eastern Alps During the Ice Ages). Populärwissenschaftliche Veröffentlichungen. Geologische Bundesanstalt. Vienna, 24 pp.

Husen van, D., 2000. Geological Processes during the Quarternary. Mitteilungen der Österreichischen Geologischen Gesellschaft, 92, 135-156.

Journel A. G. and Alabert F., 1989. Non-Gaussian data expansion in the earth sciences. Terra Nova, 1, 123-34.

Journel, A. G., 1983. Nonparametric estimation of spatial distributions. Journal of the International Association for Mathematical Geology, 15(3), 445-468.

Klingbeil, R., Kleineidam, S., Asprion, U., Aigner, T. and Teutsch, G.,1999. Relating lithofacies to hydrofacies: outcrop-based hydrogeological characterisation of Quaternary gravel deposits. Sedimentary Geology, 129(3–4), 299-310.

Krainer, K. and Poscher, G., 1992. Sedimentologische Beobachtungen im Gletschervorfeld der Pasterze (Glocknergruppe, Hohe Tauern). Carinthia II, 182/102, 317- 343.

Krige, D. G. (1951). A statistical approach to some basic mine valuation problems on the Witwatersrand. Journal of the Chemical, Metallurgical and Mining Society of South Africa, 52 (6), 119-139.

Isaaks, E. H. and Srivastava, R. M.,1989. An Introduction to Applied Geostatistics. Oxford University Press, New York, 561 pp.

Lark, R.M., 2000. A comparison of some robust estimators of the variogram for use in soil survey. European Journal of Soil Science, 51, 137-157.

Linzer, H. G., Decker, K., Peresson, H., Dell'Mour, R. and Frisch, W., 2002. Balancing lateral orogenic float of the Eastern Alps. Tectonophysics, 354(3–4), 211-237.

Poscher, G., 1994. Bericht 1993 über geologische Aufnahmen im Quartär auf Blatt 123 Zell am See. Jahrbuch der Geologischen Bundesanstalt, 3, 503-504.

Preusser, F., Reitner, J. and Schlüchter, C., 2010. Distribution, geometry, age and origin of overdeepened valleys and basins in the Alps and their foreland. Swiss Journal of Geosciences, 103(3), 407-426.

Reitner, J.M., 2007. Glacial dynamics at the beginning of Termination I in the Eastern Alps and their stratigraphic implications. Quaternary International, 164-165, 64-84.

Remy, N, 2004. Geostatistical Earth Modeling Software: User's Manual. Stanford University, CA, 85 pp.

Remy, N, Boucher, A. and Wu, J. 2009. Applied geostatistics with SGeMS: a user's guide. Cambridge, UK: Cambridge University Press, 264 pp.

Sil, S., Srinivasan, S. and. Sen, M.K. 2008. Markov Bayes simulation for structural uncertainty estimation. Proceedings of the conference of the Society of Petroleum Geophysicists (SPG), Hyderabad, Paper No. 200, 6 pp.

Strebelle S., 2000. Sequential simulation drawing structures from training images. PhD Thesis, Stanford University, USA, 374 pp.

Strebelle S., 2002. Conditional simulation of complex geological structures using multiple-point statistics. Mathematical Geology, 34, 1-2.

Strebelle, S., Payrazyan, K. and Caers, J., 2003. Modeling of a deepwater turbidite reservoir conditional to seismic data using principal component analysis and multiple-point geostatistics. SPE Journal, 8(3), 227-235.

Strebelle, S. and Journel, A, 2001. Reservoir modeling using multiple point statistics. 2001 SPE Annual Technical Conference and Exhibition, New Orleans, SPE Paper 71324, 11 pp.

Strebelle, S. and Zhang, T., 2004. Non Stationary Multiple Point – Geostatistical Models. In: O. Leuangthong and C.V. Deutsch, (eds.), Quantitative Geology and Geostatistics, 14, pp. 235-244.

Switzer, P., 1977. Estimation of distribution functions from correlated data. Bulletin of the International Statistical Institute, 47, 2, 123-137.

Webb, E.K., 1994. Simulating the three-dimensional distribution of sediment units in braided stream deposits. Journal of Sedimentary Research, B64, 219-231.

Zhang, T., Switzer, P. and Journel, A., 2006. Filter-Based Classification of training image patterns for spatial simulation. Mathematical Geology, 38, 63-80.

Zhu, H. and Journel, A.G., 1993. Formatting and integrating soft data: Stochastic imaging via the Markov – Bayes algorithm. In A. Soares, (ed.), Geostatistics Troia 92, 1, pp. 1-12.

Carmen JANDRISEVITS[1)*)], Robert MARSCHALLINGER[1)] & Thilo HOFMANN[2)]

[1)] Doctoral College GIScience, Interfaculty Department of Geoinformatics_Z-GIS, University of Salzburg, Schillerstraße 30, 5020 Salzburg, Austria;

[2)] Department of Environmental Sciences, University of Vienna, Althanstraße 14 UZA II, 1090 Vienna, Austria;

[*)] Corresponding author, carmen.jandrisevits@sbg.ac.at